Relaxation effects in thermoelastically generated ultrasound in stressed dielectric and conductive materials

A. L. Glazov ⬤* and K. L. Muratikov ⬤
Ioffe Institute, St. Petersburg 194021, Russia

In this paper, we demonstrate that the standard theory of thermoelasticity fails in describing stress dependence of laser-exited ultrasound in real dielectric and especially conductive materials. A theoretical model of thermoelasticity considering the thermal perturbation of nonstationary defect states with relaxation is presented and analyzed. To explain the obtained experimental data for metals, it is necessary to also consider a change in the pressure of the electron gas due to the defect perturbation. The proposed model is used to describe linear and nonlinear behavior of the laser ultrasonic signals near a hole in a dielectric ceramic and a metal alloy submitted to a uniform compression. The model introduces an effective dynamic coefficient of thermal expansion for real stressed materials. The obtained results provide an opportunity to estimate mechanical stresses in different materials. In this paper, we describe the calibration of the laser ultrasonic signals on stress in combination with hole drilling. The approach also allows us to estimate relaxation times of the laser-excited defects in stressed materials.

I. INTRODUCTION

In materials with a complex multicomponent structure, dynamic deformation, excitation of acoustic vibrations, and propagation of waves are often characterized by the appearance of special properties that cannot be explained with the standard theory of elasticity. In disordered materials, it is often necessary to consider relaxation processes in their defect subsystems [1–3]. To study and explain wave propagation properties of such materials, a special approach called *slow dynamics* has been developed [4,5]. Over the years, attention has been paid to the development of slow dynamic methods for studying the features of mechanical processes in heterogeneous and defective materials [6,7]. Slow dynamics helped to explain the wide range of dynamic deformation processes in materials and objects with a complex internal structure, a characteristic feature of which is the presence of relaxation processes. Such materials include complex glassy structures [8–10], ceramics [6,11], geological media [12–14], and cement [15,16]. Recently, similar behavior has been observed in the phenomena of creep [17] and contact phenomena in metals [7] and in metal alloys [18]. The phenomena of slow dynamics turn out to be quite diverse and manifest themselves on various spatial scales from nano- to meso- and macrolevels, which ensured their wide applications for diagnostics of various inhomogeneous materials [19–21].

Usually, studies carried out within the framework of slow dynamics cover elastic properties of materials, while thermal and thermoelastic ones do not receive much attention. Insufficient attention was also paid to the investigation of stressed materials with relaxation properties, while their study is of particular interest from both fundamental and practical points of view. It may result in the development of effective nondestructive, noncontact methods for assessing full-field residual stress information. It is known that the influence of stresses on the elastic characteristics of materials without relaxation processes leads to several acoustoelastic effects [22,23]. These effects are usually small and do not exceed a few percent. It was also shown in Ref. [21] that the effect of deformation on the speed of sound is several units per thousand for polycrystalline metals with multirelaxation processes with relaxation times in the range of 10^{-4} to 10^4 s. As for thermal processes, it is known from our experiments on studying areas near crack tips in silicon nitride ceramics [24,25] and experiments with metals and metal alloys [26,27] that stress has a weak effect on thermophysical parameters of materials. This influence results in the appearance of a weak anisotropy of the thermal conductivity of a material and in the phase shift of the thermal wave signal by several degrees [28].

Our experimental results on stressed materials with relaxation presented in the experimental sections of this paper demonstrate significantly stronger influence of stresses on parameters of laser ultrasound (LU) signals generated by thermoelastic mechanisms. These signal variations could reach 100% of the average signal level, and signal phase changes could exceed 100°. Thus, the effects associated with the stress influence on the elastic and thermophysical properties of materials can hardly be useful for explaining our experimental results. In this regard, the main focus of this paper is on studying the stress dependence of the thermal expansion coefficient that determines thermoelastic processes in materials. The relaxation behavior of a material due to some disorder of its structure is considered to explain noticeable phase delays of the LU signals relative to the exciting laser radiation. The results obtained can be useful in expanding the slow dynamic

*Corresponding author: glazov.holo@mail.ioffe.ru

approaches to investigation of thermoelastic processes occurring during the generation and propagation of acoustic waves in materials with the relaxation of nonstationary defects.

For a better understanding of the results obtained, let us first consider the generalized Thompson thermoelastic effect which is widely used for residual stress evaluation in materials. It considers the dependence of mechanical parameters of a material on temperature. The corresponding method is called thermoelastic stress analysis (TSA). It has been developed for various materials and objects [29]. The idea of the method is based on detecting the local variations of the surface temperature of a stressed sample under the action of periodical external loads. The interpretation of the TSA experimental data is usually carried out within the thermodynamic approach [30], in which the presence of uniaxial stresses σ in a material can be considered by introducing the effective coefficient of thermal expansion:

$$\alpha_{\text{eff}} = \alpha_0 - \frac{1}{E^2}\frac{\partial E}{\partial T}\sigma, \tag{1}$$

where α_0 is the coefficient of linear thermal expansion for the undeformed state, and E is Young's modulus of the material. Since $\partial E/\partial T < 0$ for practically all materials, in accordance with Eq. (1), the presence of tensile stress ($\sigma > 0$) in a material always leads to an increase in the coefficient of thermal expansion, whereas compression ($\sigma < 0$) leads to its decrease.

In this paper, the peculiarities of the generation of ultrasonic waves and vibrations in stressed dielectric and conductive solids with a defect subsystem are experimentally and theoretically investigated. The experiments were carried out considering the situation in which the acoustic wavelength significantly exceeds the thermal wavelength and sample size. In this case, in accordance with the results reported in Refs. [31,32], the LU signals from the samples can be considered proportional to the local value of the thermal expansion coefficient in the irradiated region of the sample. The relationship between the LU signals from a sample in free and stressed states in the frequency domain is

$$S(\vec{r}, \omega) = \frac{\alpha(\vec{r})}{\alpha_0}S_0(\vec{r}, \omega), \tag{2a}$$

or for the case of the linear dependence of the coefficient of thermal expansion on stress:

$$S(\vec{r}, \omega) = (1 + b\sigma)S_0(\vec{r}, \omega), \tag{2b}$$

where $\vec{r}$ is the radius vector of the center of the laser beam on the surface, ω is the cyclic modulation frequency of laser radiation, S_0 is the LU signal, and σ is the first stress invariant. Note that, within the framework of the thermodynamic approach, in accordance with Eq. (1), the coefficient b is

$$b = -\frac{1}{\alpha_0 E^2}\frac{\partial E}{\partial T}. \tag{3}$$

Earlier, in works on Vickers-indented ceramics [24,25,33] and metals [26,34], we have found the strong influence of residual and external stresses on LU signals. However, it was impossible to quantitatively relate the experimental signal to

the residual stresses due to the complex geometry of the indented zones and the stress distribution close to them. In this paper, experiments were performed on model samples with a round hole. A predictable stress field was induced in the samples by a controllable external load. The availability of precise analytical solutions for the distribution of stresses in such samples [35] allowed us to reveal the quantitative correlation between the experimental signal and internal stress and consequently to check the dependence of the coefficient of thermal expansion on stresses. To elucidate the specific features of the LU signals in stressed materials of different natures, experiments were performed on dielectric materials (ceramics) and on conducting materials (metal). To explain the results obtained, a slow dynamic model of thermoelastic excitation of ultrasound considering the presence of relaxation of defect states in real materials was proposed and analyzed.

II. MATERIAL PREPARATION AND EXPERIMENTAL SETUP

Experiments were carried out on samples made from two different materials: nonconductive silicon nitride ceramic NC 132 and aluminum alloy D16 (analogue 2024). Rectangular plates with a small round blind hole, i.e., a hole with a depth less than the plate thickness, in the center were chosen as model objects. In the silicon nitride ceramic, a hole was made in the center of the large face using a CO_2 laser. The hole diameter on the surface was 0.6 mm, and the depth was 0.5 mm. In D16 alloy, a hole of 0.26 mm in diameter and 0.4 mm in depth was also drilled in the center of the large face. Under uniaxial loading, the stress distribution in such an object is known analytically.

The Si_3N_4 ceramic was made by hot pressing in the direction perpendicular to the face where the hole was made. It was chosen as a dielectric material. The investigated specimen was $8.5 \times 8.1 \times 2.4\,\text{mm}^3$ in size. The surface with the hole has been polished. D16 aluminum alloy was chosen as a conductive material. The specimen size was $8.9 \times 6.9 \times 4.0\,\text{mm}^3$. The surface was finally ground with aluminum oxide grinding powder with an average particle size of 1 μm.

Ultrasonic vibrations in the samples were generated by 532 nm laser radiation modulated in time and focused on the surface of the samples. The modulated radiation power on the sample surface was 8 mW. The laser spot diameter was 12 μm. A round piezoelectric transducer of 25 mm in diameter and 5 mm in height made from lead zirconate titanate was used as a detector of ultrasonic waves at the opposite side of the samples. The detector was coupled to the sample surface with a thin layer of glycerol-based acoustic contact gel. The operating frequency was chosen close to the minimum natural resonant frequency of the transducer of 101.4 kHz.

The main idea of the experimental research in this paper was to study the dependence of the excited acoustic waves on mechanical stress. To this purpose, a uniaxial compressive load was applied to the lateral sides of the samples, which were placed between two jaws subjected to a compressive load. As a result of the action of external uniaxial stress, nonuniform stress fields with a predictable distribution were formed around the holes. For the data acquisition, the signal from the piezoelectric transducer was fed through a
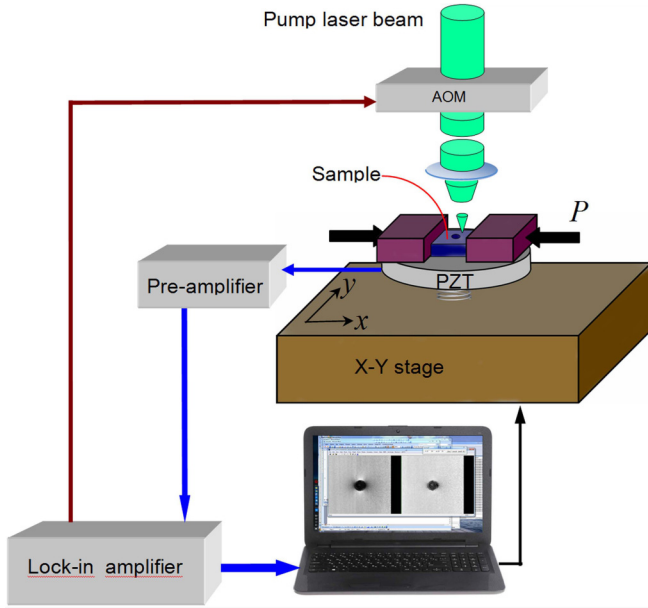
FIG. 1. Experimental set-up. AOM is the acousto-optic modulator, PZT is the piezoelectric transducer.

FIG. 2. The field of the first stress invariant around a hole under uniaxial unit compression.

preamplifier to a lock-in amplifier and then collected by a computer. The general scheme of the setup is shown in Fig. 1. The LU images of the samples were formed by two-dimensionally (2D) scanning the position of the focused laser beam on a surface. All experiments with external loads were carried out in the range of elasticity of materials. The absence of plastic deformations in the samples during the experiment was controlled by the coincidence of the LU images near the hole before and after loading.

Thermal waves excited at the modulation frequency decayed rapidly at distances of 10 μm for silicon nitride and 20 μm for aluminum alloy. Then the spatial resolution determined by the size of the laser spot and the thermal wavelength was ~30 and 50 μm, respectively.

III. EXPERIMENTAL RESULTS

A. Introduction into the Kirsch problem: Stress distribution around a hole

Let us consider in more detail the stress disturbance near a hole. For a plate with a through-hole subjected to the uniform load P along the line with $\varphi = 0$, the radial and circumferential stresses σ_r and σ_φ around the hole are found using the expressions [35]:

$$\sigma_r(r, \varphi) = \frac{P}{2}\left(1 - \frac{a^2}{r^2}\right) + \frac{P}{2}\left(1 + \frac{3a^4}{r^4} - \frac{4a^2}{r^2}\right)\cos 2\varphi, \quad (4)$$

$$\sigma_\varphi(r, \varphi) = \frac{P}{2}\left(1 + \frac{a^2}{r^2}\right) - \frac{P}{2}\left(1 + \frac{3a^4}{r^4}\right)\cos 2\varphi, \quad (5)$$

where r is the radial distance, the polar angle φ is measured as shown in Fig. 2, and a is the hole radius. In this case, the radial stress on the inner surface of the hole is equal to zero,
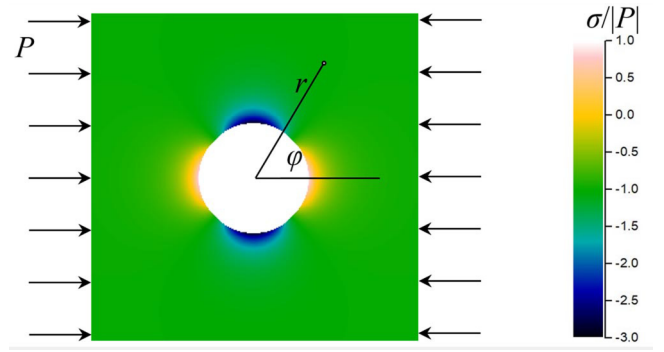
i.e., $\sigma_r(a, \varphi) = 0$, and the circumferential stress have maxima and minima:

$$\sigma_\varphi(a, 0) = \sigma_\varphi(a, \pi) = -P,$$

$$\sigma_\varphi\left(a, \frac{\pi}{2}\right) = \sigma_\varphi\left(a, -\frac{\pi}{2}\right) = 3P.$$

The first invariant of the stress tensor near the surface is determined by the equality:

$$\sigma = \sigma_r + \sigma_\varphi = P - P\frac{2a^2}{r^2}\cos 2\varphi, \quad (6)$$

where it is considered that, on the surface, $\sigma_z = 0$. Figure 2 shows the stress distribution σ around the hole for the uniaxial compression in the form of a 2D color map.

Strictly speaking, Eq. (6) describes the behavior of stresses around a through-hole in sufficiently thick plates. Under the experimental conditions, the thermoelastic generation of the acoustic waves occurred in a thin near-surface region of the sample. In accordance with the work by Folias and Wang [36], the stress on the surface and in the bulk may differ by 15% for the ratios of the hole radius to the plate thickness mentioned in Sec. II, but the stress distribution around the hole remains close to that given by Eq. (6). Therefore, this difference is not considered further, and the analysis of the obtained experimental data will be carried out using Eq. (6).

Substituting Eq. (6) into Eq. (2a), we obtain the assumed theoretical dependence of the LU signal on the applied load in the form:

$$S = S_0\left(1 + bP - bP\frac{2a^2}{r^2}\cos 2\varphi\right). \quad (7)$$

B. Ceramic sample

First, we experimentally examine the ceramic sample. Figure 3(a) shows the LU image of the area around the hole in the unloaded sample. The signal distribution is almost uniform. Figures 3(b) and 3(c) depict the same part of the sample under the loads of −16 and −30 MPa. The images of the uniaxially loaded sample clearly show the strong redistribution of the signal amplitude near the hole. Moreover, the areas with increased and decreased signals have diametrically symmetrical location around the hole, as in Fig. 2.

FIG. 4. Distribution of signals corresponding to the images in Fig. 3 along a circle with a radius of 0.4 mm; black crosses for experimental data for a sample without load; blue circles for the sample under the compressive load of −16 MPa; red triangles for the sample under the compressive load of −30 MPa. The lines of the corresponding colors are fitting curves derived using Eq. (8).
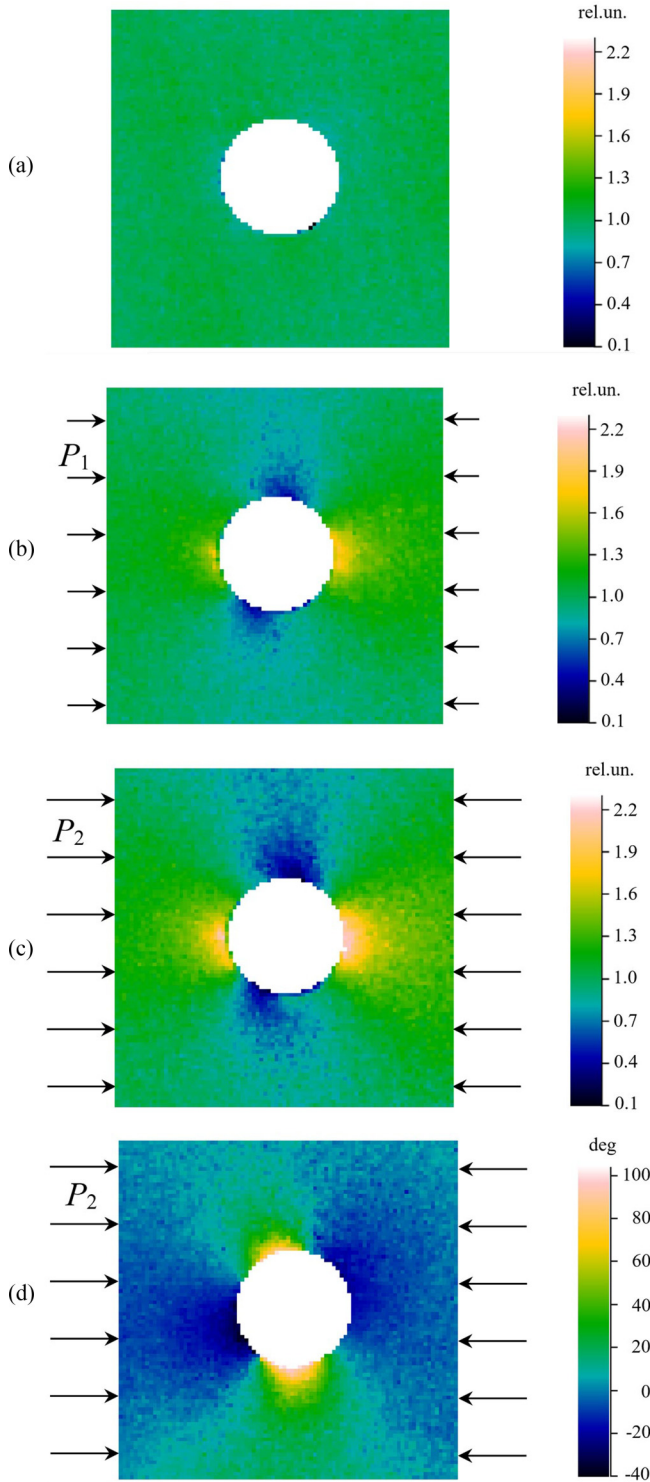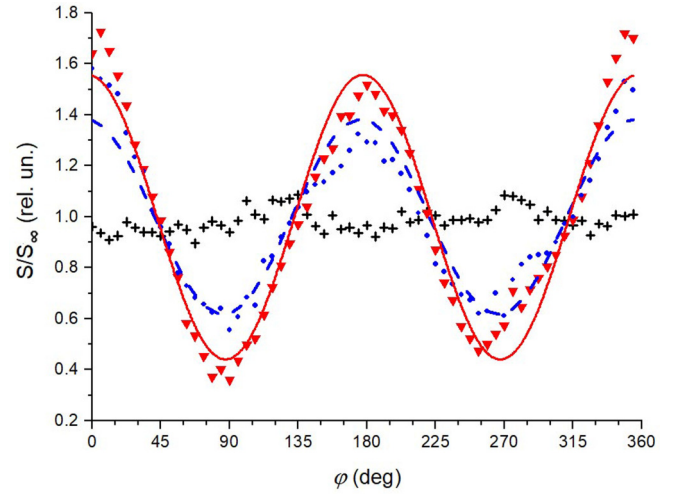
FIG. 3. Laser ultrasound (LU) images of a silicon nitride sample region. (a) The signal amplitude for the sample in the initial state. (b) The signal amplitude for sample under uniaxial compression $P_1 = -16$ MPa. (c) The signal amplitude for sample under uniaxial compression $P_2 = -30$ MPa. (d) The signal phase for sample under uniaxial compression $P_2 = -30$ MPa. The size of the images is 1.8×1.8 mm^2. The scan step is 20 μm.

From Eqs. (2a) and (3) and the data in Figs. 2 and 3, it can be seen that there is a qualitative agreement between the experimental and theoretical images; namely, the LU signal decreases in zones of compressive stresses and increases in zones of tensile stresses, in accordance with the behavior of the thermal expansion coefficient as in Eq. (2a).

For a quantitative analysis, we will approximate the LU signal from the sample under the load P by the function:

$$S = S_\infty \left\{ 1 - \frac{2bPa^2}{(1 + bP)r^2} \cos \left[2(\varphi - \varphi_0) \right] \right\}, \qquad (8)$$

with parameters S_∞, b, and φ_0 which can be used for fitting the data. Here, S_∞ is the signal far from the hole, and φ_0 is the angle between the load direction and the reference direction. For the quantitative analysis of the experimental data, a nonlinear fitting procedure was carried out according to the Levenberg-Marquardt method using OriginPro software. The fitting was performed for several images at different external loads.

Figure 4 shows the distribution of experimental signals along the circumference with the radius of 0.4 mm and the theoretical approximation derived from Eq. (8). For the silicon nitride ceramic, the results of the fit at the radius $a = 0.30 \pm 0.01$ mm are $b = 17 \pm 3$ GPa^{-1} at the load $P_1 = -16 \pm 2$ MPa and $b = 13 \pm 2$ GPa^{-1} at the load $P_2 = -30 \pm 2$ MPa.

The main uncertainty in all experiments is due to the measurement uncertainty of the applied load P and the hole radius a. The standard error of the fit was <3% in all cases. The presented results show that Eq. (8) approximates reasonably well the experimental signal for Si$_3$N$_4$ ceramics. This suggests that the amplitude of acoustic vibrations, as expected, is a function of the first stress invariant. This dependence is associated with the isotropy of sample properties on the surface and temperature fields in the region of ultrasound generation.

The stress field around a hole demonstrates strong gradients, and one can suppose that stress or strain gradient also affects the LU signal. To assess the possible influence of stress and strain gradients on the coefficient b, we analyzed the averaged data for the absolute LU signal S outside a concentric

circle of radius $r = 4a$. From Saint-Venant's principle, the hole practically does not affect the stress distribution at this distance, and we can neglect stress gradient effects. The signal amplitude demonstrated monotonic behavior in accordance with Eq. (2a). A linear fit gives $b = 13 \pm 2\,\mathrm{GPa}^{-1}$, which is in good agreement with the value obtained from the angular signal distribution near the hole. Thus, the stress and strain gradients do not noticeably affect the LU signal.

For the silicon nitride ceramic studied in this paper, $\partial E/\partial T = -0.014\,\mathrm{GPa\,K}^{-1}$ [37], $\alpha_0 = 3.3 \times 10^{-6}K^{-1}$, the average Young's modulus $E = 315\text{–}320\,\mathrm{GPa}$ [38], and thus, in accordance with thermodynamic result [Eq. (1)], in the zones of uniaxial stresses, the thermal expansion coefficient should depend on the stress as

$$\alpha \approx \alpha_0(1 + 0.043[\mathrm{GPa}^{-1}]\sigma). \qquad (9)$$

Thus, the experimentally found average value of the coefficient b turns out to be much larger than the theoretical value of the similar coefficient determined by Eq. (3) which considers only the thermodynamic dependence of the elastic modulus on temperature. The large discrepancy in the values of the coefficients of the linear dependence on stress indicates the presence of an additional mechanism that affects the coefficient of thermal expansion along with the dependence of the elastic modulus on temperature.

Above, we considered the behavior of the LU signal magnitude, which only quantitatively differs from that predicted by classical thermodynamics. More surprising, however, is the behavior of the LU signal phase. According to Eq. (2a), the phase of the signal does not depend on stress. Figure 3(d) presents the phase distribution of the LU signal around the hole at the external compressive load of -30 Mpa. The distribution shows a clear relationship between phase and stress. The phase changes by $\sim 140°$ with an increase in stress from -90 to 30 Mpa.

In Sec. IV, we discuss some theoretical arguments confirming the existence of the slow dynamic mechanism in investigated stressed samples, which help to explain the obtained experimental data.

C. Metal sample

Let us now consider the excitation of acoustic vibrations in a stressed metal sample. Anomalous slow dynamic acoustic effects were previously observed in aluminum alloys [18]. Elastic properties of a material like the D16 aluminum alloy analyzed here were reported in Ref. [39], $E = 73\,\mathrm{GPa}$, $\partial E/\partial T = -0.042\,\mathrm{GPa\,K}^{-1}$, and $\alpha_0 = 23 \times 10^{-6}K^{-1}$. Substituting these values in Eqs. (1) and (2a), we expected a positive value for b : $b \approx 0.34\,\mathrm{GPa}^{-1}$.

The LU images of the area around the hole in the D16 aluminum alloy in the initial state and under load are shown in Fig. 5. Figure 5(a) shows that the image of the sample in the initial state presents a characteristic distribution of the LU signal around the hole, which indicates the presence of residual stress in the sample. The comparison of the LU images of the loaded metallic sample with similar images for ceramics

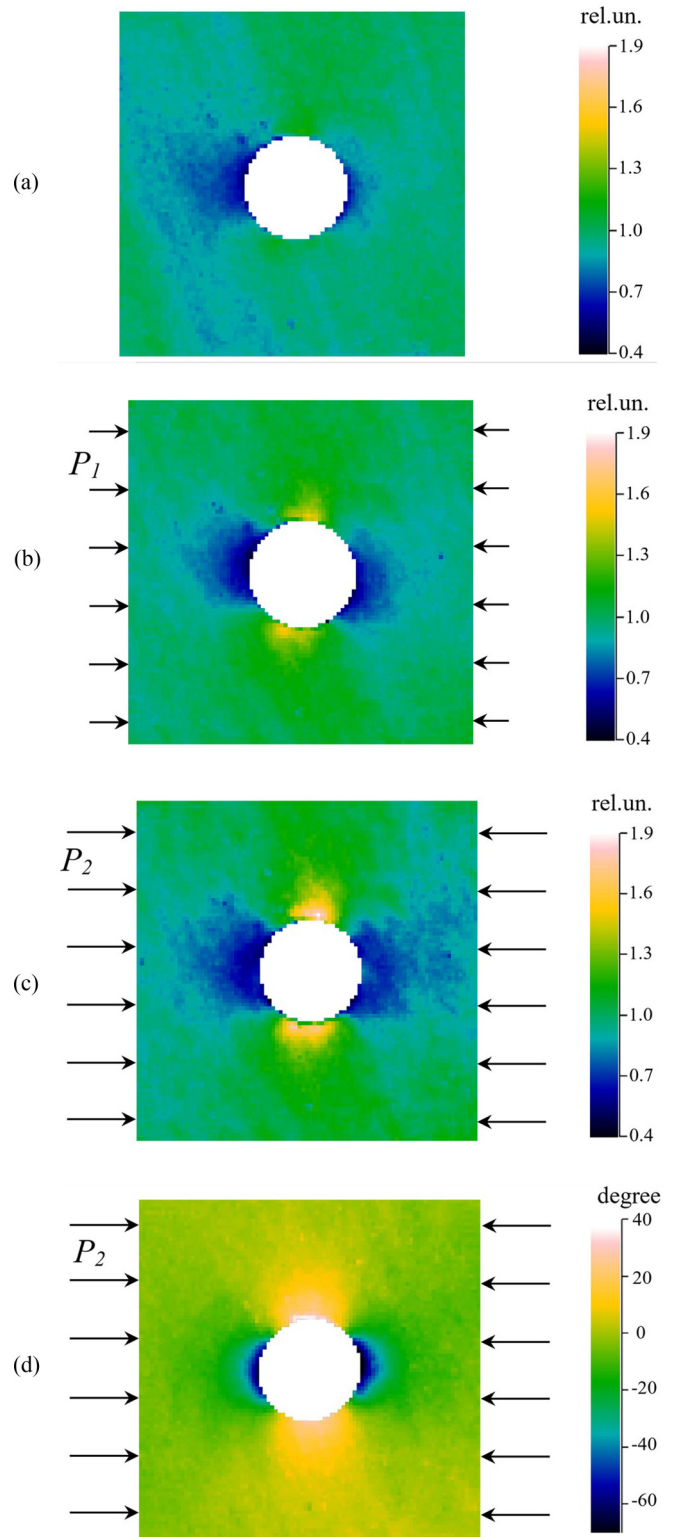FIG. 5. Laser ultrasound (LU) images of the sample area for the D16 aluminum alloy. (a) The sample in the initial state. (b) The sample under compression $P_1 = -21\,\mathrm{MPa}$. (c) The sample under compression $P_2 = -34\,\mathrm{MPa}$. (d) The signal phase for sample under uniaxial compression $P_2 = -34\,\mathrm{MPa}$. The size of the images is 0.9×0.9 mm. Scan step is $10\,\mu$m.
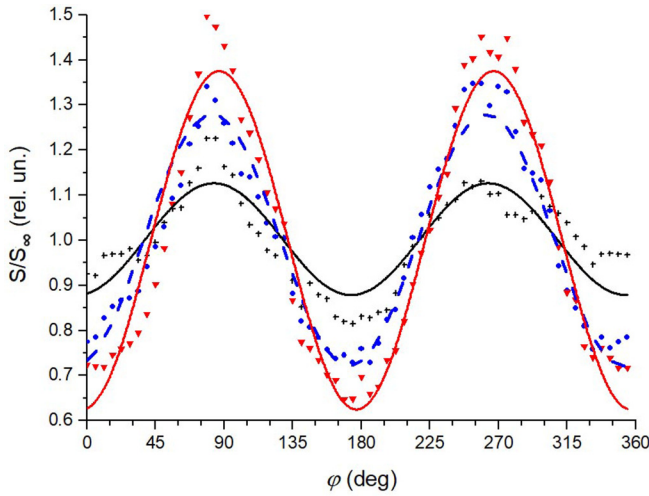
FIG. 6. Distribution of the signals corresponding to the images in Fig. 5 along a circle with the radius of 0.2 mm. Black crosses are experimental data for the sample without loading; blue circles for the sample under the compressive load of -21 MPa; red triangles for the sample under the compressive load of -34 MPa. The lines of the corresponding colors are fitting curves according to Eq. (8).

shows that the LU signal changes in the opposite way under the load, namely, it increases in zones with compressive stresses and decreases in zones with tensile stresses.

The experiment with an external load makes it possible to determine the coefficient b if the residual stress σ' in the sample far from the hole in the initial state is also uniaxial. The residual stress distribution could be due to two alternative cases: compressive stress along the direction $\varphi = 0$ or tensile stress along the direction $\varphi = \pi/2$. This ambiguousness will slightly affect b. In the following, we will consider only the first case, i.e., that of compressive residual stress. For signal approximation, we use two equations in the form of Eq. (8) for the initial and loaded states. The fitting procedure is the same as described in Sec. III B. The fit results are $b = -15 \pm 6 \, \mathrm{GPa}^{-1}$ and $\sigma' = -12 \pm 2 \, \mathrm{MPa}$ for the load $P_1 = -21 \pm 2$ MPa and $b = -22 \pm 11 \, \mathrm{GPa}^{-1}$ and $\sigma' = -10 \pm 2 \, \mathrm{MPa}$ for the load $P_2 = -34 \pm 2$ MPa. Figure 6 shows the distribution of experimental signals along the circumference with the radius of 0.2 mm and the theoretical approximation derived from Eq. (8). Thus, in accordance with the experiment, in both cases, the coefficient b is negative, and its absolute value is much larger than predicted by the thermodynamic theory. For the case of tensile residual stress σ' along the direction $\varphi = \pi/2$, the fitting procedure gives a slightly different value of the coefficient b, but its sign is still negative. As will be shown in the theoretical Sec. IV, the dependence of the coefficient of thermal expansion on stress is nonlinear, which resulted in slightly different estimated values of the coefficients b for different loads.

With increasing load on the sample, an increase of the signal is observed in the regions where a minimum is theoretically expected. To explain the discrepancy, a deviation from the linear dependence on stress must be considered by adding a quadratic term in Eq. (2a):

$$S(\vec{r}, \omega) = \left(1 + b\sigma + c\sigma^2\right) S_0(\vec{r}, \omega). \tag{10}$$
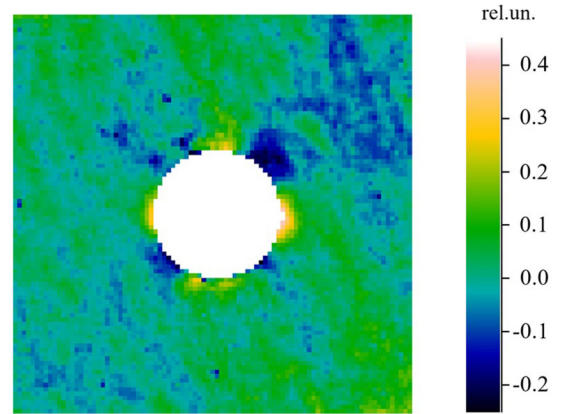

FIG. 7. Residuals for fitting the laser ultrasound (LU) image of the area of the sample from D16 aluminum alloy under the uniaxial load of -34 MPa. The image size is 0.9×0.9 mm. Scan step is $10 \, \mu$m.

The expression for the stress distribution [Eq. (6)] becomes

$$S(r, \varphi) = S_0 \Bigg[1 + bP + cP^2 \left(1 + \frac{2a^4}{r^4}\right) - 2(bP + 2cP^2)$$
$$\times \frac{a^2}{r^2} \cos 2\varphi + 2cP^2 \frac{a^4}{r^4} \cos 4\varphi \Bigg]. \tag{11}$$

Figure 7 shows residuals when approximating the experimental image using Eq. (8), that is, considering only the linear dependence. The 2D residual distribution clearly shows four maxima around the hole, corresponding to a term proportional to $\cos(4\varphi)$. As can be seen from Eq. (11), this term decreases as r^{-4}. Therefore, it appears much closer to the edge of the hole. The experimental data for the signal along circles with radii of 0.16 and 0.2 mm are shown in Fig. 8(a). Fitting curves obtained in accordance with Eqs. (8) and (11) are also shown there. The points in Fig. 8 represent the residuals when a signal is approximated by a linear dependence [Eq. (8)] and approximation of the residuals by the function proportional to $\cos(4\varphi)$. Thus, at moderate stresses, a noticeable nonlinear component of the dependence of the LU signal on stress for the D16 alloy is observed. Considering the quadratic term when approximating the signal leads to an insignificant change in the coefficient b and makes it possible to determine the coefficient c. Assuming the presence of compressive stress along the direction $\varphi = 0$ in the unloaded sample, we get $b = -16 \pm 7 \, \mathrm{GPa}^{-1}$ and $c = 400 \pm 200 \, \mathrm{GPa}^{-2}$. Since the coefficient c is positive, both compressive and tensile stresses lead to an increase of the nonlinear LU signal. The specific feature of the observed type of nonlinearity is that it appears at the modulation frequency, whereas classical thermodynamics predicts nonlinear dependence on stress only at higher harmonics [40].

For the aluminum sample, we also analyzed the absolute signal at a distance of four hole radii from the center of the hole. The obtained coefficient of linear dependence on load is $b = -16 \pm 1 \, \mathrm{GPa}$ which, as in the case of the ceramic sample, corresponds to the values obtained during the previous experiment.
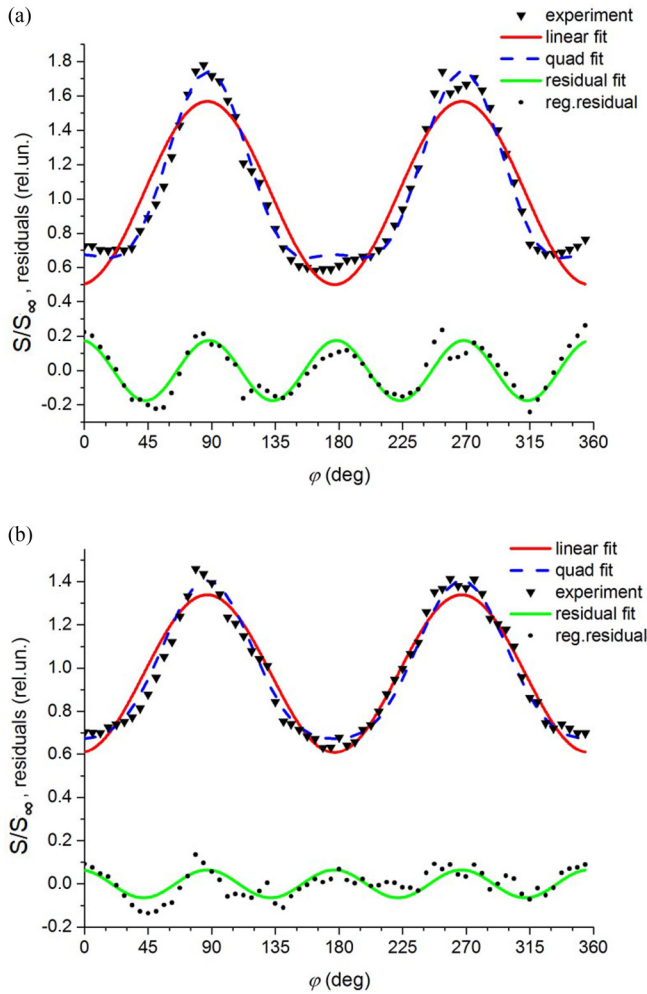
(a)

(b)

FIG. 8. (a) Distribution of the signal corresponding to the image of the sample under the compressive load of -34 MPa in Fig. 5 along a circle with the radius of 0.16 mm; black triangles for experimental data; red solid curve is a fitting curve for the linear dependence of the signal on stress; blue dashed curve is a fitting curve for the square-law dependence of the signal on the stress; black circles for residuals at linear fit; green solid curve is the difference between the fitting blue and red curves. (b) The same as (a) but detected on a radius of 0.2 mm. We recall that the hole radius in the aluminum alloy sample was of 0.13 mm.

IV. THEORETICAL MODELING ANALYSIS

This section presents the modified theory of thermoelastic generation of ultrasonic vibrations in stressed imperfect solids to explain the observations reported before and the discrepancy with respect to the expected theoretical value for b. The proposed approach is based on the slow dynamic concepts. The slow dynamic approach describes the material behavior based mainly on the defect subsystem change under various external actions. Vakhnenko et al. [41,42] proposed a general kinetic equation for the dynamics of a defect subsystem within the framework of slow dynamics. They introduced two distributions of energy barriers for the activation and deactivation of a defect that are characterized by two different times. These times depend generally on the activation energies and

temperature. To explain the experimental results, we need to determine a function of the defect activation in the material.

When analyzing the problems of fracture of stressed materials, Zhurkov [43] and Zhurkov and Korsukov [44] obtained good results by choosing the following expression for the probability rate of the defect activation:

$$p = \frac{1}{\tau_0} \exp\left(-\frac{U - \Omega\sigma}{k_b T}\right), \qquad (12)$$

where τ_0 is the oscillation period or inverse Debye frequency ($\tau_0 \approx 0.1$ ps), U is the energy of the defect activation, σ is the first invariant of the mechanical stress tensor in the case of an isotropic material, Ω is the activation volume of the defect, κ_b is the Boltzmann constant, and T is the local absolute temperature of the material. Note here that Zhurkov studied the lifetime of solid samples by applying uniaxial quasistatic tension, that is, assuming $\sigma > 0$.

In our experiments, LU was generated due to local variation of the sample temperature produced by the laser radiation. The laser power was too weak to generate new defects in the sample: the generation time of a vacancy in aluminum by a weak thermal effect of radiation is on the order of 10^{-3} s [45], which is much longer than the period between the laser pulses at the used modulation frequencies of $\sim$100 KHz. Therefore, we will assume that defects in the samples were already present before the measurements. Notice that, since we performed the experiments with compressive loading, we should change the sign before σ in Eq. (12). Then we can write the local defect concentration $n_\sigma^{(d)}$ in the stressed samples as

$$n_\sigma^{(d)} = n^{(d)} \exp\left(-\frac{U + \Omega\sigma}{k_b T_0}\right), \qquad (13)$$

where $n^{(d)}$ is the concentration of potential defects in the material when the activation barrier U is fully compensated by stress, σ is the total stress distribution forced in the sample by an external load and possible residual stress, and T_0 is the absolute temperature of the sample before laser exposure.

In Refs. [41,42], a kinetic equation for local relaxation events was proposed with two relaxation times that consider an essential asymmetry in processes of rupture and recovery of intergrain cohesive bonds in sedimentary rocks. When considering stress relaxation processes in liquids as an elastic medium, a kinetic equation with one relaxation time was proposed [46]. We assume that (i) the concentration of defects in the investigated ceramic and metal samples is low enough to neglect the interaction between them, (ii) defects are localized, and (iii) there is no diffusion process under laser exposure. Under these conditions for local relaxation events of excited defects, the kinetic equation for concentration Δn_σ can be written in a simple general form [46]:

$$\frac{\partial \Delta n_\sigma}{\partial t} + \frac{\Delta n_\sigma}{\tau} = G(\vec{r}, t), \qquad (14)$$

where $\tau = \tau_0 \exp[(U + \Omega\sigma)/k_b T_0]$ is the relaxation time of the excited defect, and $G(\vec{r}, t)$ is the generation function.

Let us suppose that the initial concentration of defects in the material is created by applying an external stress to the sample. A change in temperature under laser irradiation leads additionally to a change in the value of the activation

energy U of the defect at temperature T_0 to a new value U' at temperature T which is related with U by a linear expression $U' \approx U + 3\alpha_0 \Omega \sigma \Delta T$, where $\Delta T = T - T_0$. By considering these assumptions, the function $G(\vec{r}, t)$ may be represented by the relation:

$$
\begin{aligned}
G(\vec{r}, t) &= \frac{n_\sigma^{(d)}}{\tau_0} \left[\exp\left(-\frac{3\alpha_0 \Omega \sigma \Delta T}{k_b T_0} \right) - 1 \right] \\
&= \frac{n_0^{(d)}}{\tau_0} \exp\left(-\frac{\Omega \sigma}{k_b T_0} \right) \left[\exp\left(-\frac{3\alpha_0 \Omega \sigma \Delta T}{k_b T_0} \right) - 1 \right],
\end{aligned}
\tag{15}
$$

where the concentration $n_0^{(d)} = n^{(d)} \exp(-U/k_b T_0)$ corresponds to the unstressed state of the sample with $\sigma = 0$.

When the condition $3\alpha_0 \Omega \sigma \Delta T \ll k_b T_0$ is satisfied, the kinetic equation for Δn_σ can be linearized, and it takes the form:

$$
\frac{\partial \Delta n_\sigma}{\partial t} + \frac{\Delta n_\sigma}{\tau} = -\frac{n_0^{(d)}}{\tau_0} \exp\left(-\frac{\Omega \sigma}{k_b T_0} \right) \frac{3\alpha_0 \Omega \sigma}{k_b T_0} \Delta T. \tag{16}
$$

In Eq. (16), Δn_σ depends on the spatial coordinates through σ, τ, and ΔT. However, going back to the experimental conditions, the temperature variations at the used frequencies in the sample occurred at distances significantly smaller than those over which stress varies around the holes. Therefore, σ and τ can be considered slowly varying functions of coordinates in comparison with ΔT. A solution of Eq. (16) is

$$
\begin{aligned}
\Delta n_\sigma = &-\frac{n_0^{(d)}}{\tau_0} \frac{3\alpha_0 \Omega \sigma}{k_b T_0} \exp\left(-\frac{\Omega \sigma}{k_b T_0} \right) \\
&\times \int_{-\infty}^{t} dt' \exp\left(-\frac{t - t'}{\tau} \right) \Delta T(\vec{r}, t').
\end{aligned}
\tag{17}
$$

According to Kosevich [47], the presence of defects with the concentration n_σ in the material lattice leads to a change of its free energy:

$$
\Delta F = K\Omega \Delta n_\sigma u_{ii}, \tag{18}
$$

where $K = \lambda + 2\mu/3$ is the modulus of uniform compression, λ and μ are Lamé coefficients, and u_{ik} is the deformation tensor. As usual, repeated indices indicate summation. It follows that the equation of state of the material in the presence of defects can be written in the form:

$$
\sigma_{ij} = \sigma_{ij}^{(el)} - K(3\alpha_0 \Delta T - \Omega \Delta n_\sigma) \delta_{ij}, \tag{19}
$$

where $\sigma_{ij}^{(el)} = \lambda u_{kk} \delta_{ij} + 2\mu u_{ij}$, and δ_{ik} is the Kronecker delta.

Deformations in the material with the stress tensor given by Eq. (19) are obtained from the equation of motion:

$$
\rho \frac{\partial^2 u_i}{\partial t^2} = \frac{\partial \sigma_{ik}^{(el)}}{\partial x_k} - K\left(3\alpha_0 \frac{\partial \Delta T}{\partial x_i} - \Omega \frac{\partial \Delta n_\sigma}{\partial x_i} \right), \tag{20}
$$

with $\vec{r} = (x_1, x_2, x_3)$.

Since Δn_σ is determined by Eq. (17), the equation of motion becomes

$$
\begin{aligned}
\rho \frac{\partial^2 u_i}{\partial t^2} = &\frac{\partial \sigma_{ik}^{(el)}}{\partial x_k} - 3\alpha_0 K\left[\frac{\partial \Delta T(\vec{r}, t')}{\partial x_i} + \Omega^2 \frac{n_0^{(d)}}{\tau_0} \frac{\sigma}{k_b T_0} \right. \\
&\times \exp\left(-\frac{\Omega \sigma}{k_b T_0} \right) \int_{-\infty}^{t} dt' \exp\left(-\frac{t - t'}{\tau} \right) \\
&\left. \times \frac{\partial \Delta T(\vec{r}, t')}{\partial x_i} \right].
\end{aligned}
\tag{21}
$$

Assuming a harmonic law of the temperature variations due to the laser action $\Delta T(t) = \Delta \tilde{T}(\omega) \exp(i\omega t)$ as expected from the experimental conditions, the equation of motion can be written as

$$
\begin{aligned}
-\rho \omega^2 \tilde{u}_i = &\frac{\partial \tilde{\sigma}_{ik}^{(el)}}{\partial x_k} - 3\alpha_0 K\left[\frac{\partial \Delta \tilde{T}(\vec{r}, \omega)}{\partial x_i} + \Omega^2 \frac{n_0^{(d)} \tau}{\tau_0} \frac{\sigma}{k_b T_0} \right. \\
&\left. \times \frac{1}{1 + i\omega\tau} \exp\left(-\frac{\Omega \sigma}{k_b T_0} \right) \frac{\partial \Delta \tilde{T}(\vec{r}, \omega)}{\partial x_i} \right].
\end{aligned}
\tag{22}
$$

Equation (22) shows that the presence of defect states in the material can be considered by introducing an effective thermal expansion coefficient of dielectric materials in a stressed state in the presence of relaxation processes. We obtain

$$
\alpha_{\text{eff}} = \alpha_0 \left[1 + \frac{n_0^{(d)} \tau}{\tau_0} \frac{\Omega^2}{k_b T_0} \frac{\sigma}{1 + i\omega\tau} \exp\left(-\frac{\Omega \sigma}{k_b T_0} \right) \right]. \tag{23}
$$

To determine the deformations arising in conducting materials during relaxation processes, it is necessary to also consider changes in the state of the electronic subsystem. Fluctuations in the defect subsystem of a conductor may result in changes of electronic pressure. We have considered this phenomenon to explain thermoelastic vibrations of aluminum membranes [48]. For this purpose, we need to add one more term to the equation of motion:

$$
\rho \frac{\partial^2 u_i}{\partial t^2} = \frac{\partial \sigma_{ik}^{(el)}}{\partial x_k} - K\left(3\alpha_0 \frac{\partial \Delta T}{\partial x_i} - \Omega \frac{\partial \Delta n_\sigma}{\partial x_i} \right) - \frac{\partial p_e}{\partial x_i}, \tag{24}
$$

where p_e is the electronic pressure.

In metals, the electron pressure is given as

$$
p_e = \frac{2}{5} n_e E_F + \frac{\pi^2}{6} n_e E_F \left(\frac{k_b T}{E_F} \right)^2, \tag{25}
$$

where E_F is the Fermi energy, and n_e is the concentration of electrons.

The chemical bond between the metal lattice atoms is due to free conduction electrons. Electrons associated with defect structures in the lattice in the general case are in a quasilocalized state and are not included in the number of electrons filling the conduction band. The excitation of defect states of the metal lattice due to the temperature modulation is accompanied by the transition of an electron or electrons from one potential well to another [49]. Between the two quasilocalized states, such electrons behave in a quasifree manner, at least during the relaxation time τ. This behavior of electrons is confirmed by the excitation and relaxation of the electronic conductivity of highly disordered metal thin films [49]. For such films, the authors observed a slow decay of conductivity after its rise forced by a heat pulse. Based on these ideas, we

assume that a change in the concentration of excited defect states in metals is accompanied by a change in the concentration of quasifree electrons. The volume of a defect in a material coincides roughly with the volume of an elementary crystal cell [45]. Since the activation of a defect in aluminum may affect also the nearest six atoms [50] and these atoms are trivalent, we will assume $\Delta n_e \approx 18 \Delta n_\sigma$. In accordance with Eq. (26), a change in the pressure of the electron gas will take place. The estimates show that, in this case, the first term on the right-hand side of Eq. (25) significantly exceeds the second one, which could thus be considered negligible and will be neglected in our calculations. In conclusion, we obtain the following link between electron pressure variation and defects concentration variation:

$$\Delta p_e = \tfrac{2}{3} E_\mathrm{F} \Delta n_e \cong 12 E_\mathrm{F} \Delta n_\sigma. \tag{26}$$

Thus, the equation of motion in Eq. (21) needs to be modified for aluminum as

$$
\begin{aligned}
\rho \frac{\partial^2 u_i}{\partial t^2} = {} & \frac{\partial \sigma_{ik}^{(el)}}{\partial x_k} - 3\alpha_0 K \bigg[\frac{\partial \Delta T}{\partial x_i} + \Omega \frac{n_0^{(d)} \sigma}{\tau_0 k_b T_0} \\
& \times \exp\left(-\frac{\Omega \sigma}{k_b T_0}\right)\left(\Omega - 12\frac{E_\mathrm{F}}{K}\right) \int_{-\infty}^{t} dt' \\
& \times \exp\left(-\frac{t-t'}{\tau}\right) \frac{\partial \Delta T(\vec{r}, t')}{\partial x_i} \bigg].
\end{aligned}
\tag{27}
$$

The effective value of the coefficient of thermal expansion for aluminum may be determined similarly to that discussed for Eq. (22). We obtain

$$
\alpha_\mathrm{eff} = \alpha_0 + \frac{\alpha_0 \Omega n_0^{(d)} \tau}{\tau_0 k_b T_0} \exp\left(-\frac{\Omega \sigma}{k_b T_0}\right) \frac{\sigma}{1+i\omega\tau}\left(\Omega - 12\frac{E_\mathrm{F}}{K}\right).
\tag{28}
$$

With known values of α_eff, it is possible to analyze the behavior of the LU signals in stressed regions of materials. As noted above, under our experimental conditions, the LU signals are proportional to the local value of the thermal expansion coefficient. Then in the presence of relaxation in the material, the coefficients b_d for dielectric ceramics and b_c for metals (instead of the coefficient b given by Eq. (3) for classical thermoelastic theory) will be modified according to Eqs. (23) and (28). It follows

$$b_d = \frac{n_0^{(d)} \tau}{\tau_0} \frac{\Omega^2}{k_b T_0} \frac{1}{1+i\omega\tau}, \tag{29}$$

$$b_c = \frac{n_0^{(d)} \tau}{\tau_0} \frac{\Omega}{k_b T_0} \frac{1}{1+i\omega\tau}\left(\Omega - 12\frac{E_\mathrm{F}}{K}\right). \tag{30}$$

Equations (23) and (28) show that the stress dependence of α_eff for dielectrics and metals can differ significantly. The thermal expansion coefficient and the LU signal for dielectric materials always increase with an increase in tensile stress while $\sigma < k_b T_0 / \Omega$, whereas for metals, they can decrease at $E_\mathrm{F} > \Omega K / 12$. It can be seen from Eqs. (23) and (28) that, in the general case, the stress dependence of the effective thermal expansion coefficient is nonlinear. Therefore, to get the linear dependence coefficients b_d and b_c in both cases, we must assume $\Omega \sigma / k_b T_0 < 1$ and expand the exponent into a series. The expressions in Eqs. (23) and (28) also make it

possible to obtain the coefficients c for dielectrics and metals that determine the square-law dependence of the LU signals on stress:

$$c_d = -\frac{n_0^{(d)} \tau}{\tau_0} \frac{\Omega^3}{(k_b T_0)^2} \frac{1}{1+i\omega\tau}, \tag{31}$$

$$c_c = -\frac{n_0^{(d)} \tau}{\tau_0} \left(\frac{\Omega}{k_b T_0}\right)^2 \frac{1}{1+i\omega\tau}\left(\Omega - 12\frac{E_\mathrm{F}}{K}\right). \tag{32}$$

The obtained values of the coefficients b are in good agreement with the observed behavior of the LU signals for ceramics and metals vs stress in the linear approximation. They show that the different features of the LU signal behavior with stress for a metal are related to the contribution of the electron gas pressure. The obtained result for the coefficient c_c also provides a correct contribution of the quadratic part of the LU signal for metal in comparison with its linear stress dependence. They also show that the phase of the LU signals can depend strongly on stress at $\omega\tau > 1$.

V. DISCUSSION

A. Ceramics

Equations (23) and (28) allow estimating the dependence of the effective thermal expansion coefficient on stress for well-studied ceramics and metals. Let us assume that the maximal initial concentration of defects in ceramics is of the order of $n^{(d)} \cong 10^{20}\,\mathrm{cm}^{-3}$. To estimate the concentration of defects excited in ceramics due to the presence of stress, it is necessary to know the activation energy in the exponent in Eq. (13). In silicon nitride ceramics, there are defects with rather high activation energy at $\sim 2.2\,\mathrm{eV}$ [51]. According to the data from Ref. [52], defects in the bulk regions of the lattice of this ceramic are also present with lower activation energy in the range from 33.9 to 40.4 kJ mol^{-1}, which corresponds to 0.351–0.419 eV. Due to the presence of grain boundaries, cavities, and defects in silicon nitride ceramics, there is also an even lower activation energy, amounting to only 15.46–17.49 kJ mol^{-1} [52], which corresponds to 0.160–0.181 eV. For Si$_3$N$_4$ ceramics, the average grain size was of ~ 10–$20\,\mu\mathrm{m}$. If we take the thickness of the near-surface layer of ceramic grains to be about several atomic layers, then the ratio of near-surface atoms to total bulk atoms situated inside grains is $\sim 10^{-3}$. With the indicated ratio of bulk and surface defects and considering the lower values of activation energies for surface defects, it follows that the contribution of bulk and surface defects to the LU signal can be comparable. Therefore, in the following, we assume the activation energy of defects equal to 0.160 eV. The value of the exponent in the coefficient b_d at room temperature is of the order of 10^{-3}. When a defect is formed in a material, its volume is usually comparable with the volume of a lattice unit cell [45]. In silicon nitride ceramics, for the α and β phases, the volume of unit cells is $\Omega \approx 10^{-28}\mathrm{m}^3$.

In the experiments, a considerable change in the phase of the LU signals was observed for areas with different stresses, which is inconsistent with the classical thermodynamic model. The slow dynamic approach developed here explains the phase behavior through the relaxation time. As

seen in Fig. 3(d), a phase difference of $\sim 140°$ (2.44 rad) corresponds to a stress of 120 MPa. Phase 2.44 rad corresponds to $\omega\tau = 0.84$, which gives approximately $\tau \approx 10^{-6}$s. This value correlates with Eq. (23) at the specified parameters of the Si_3N_4 ceramics if we consider the period of atomic vibrations in the lattice τ_0 of the order of 10^{-13}s. However, the phase behavior of the LU signals in Fig. 3(d) shows that relaxation is faster for weaker mechanical stresses. Note that, in other works, we also observed similar amplitude and phase changes of the LU signal in zones with tensile stresses near crack tips in Si_3N_4 ceramics [24,25].

B. Metal alloy

As for metals, the activation energies can have significantly lower values. In the D16 aluminum alloy, the Al content ranges from 90.8 to 94.7%. Impurities such as Cu, Mg, Fe, Si, and other metals are present. The most typical defects for metals are vacancies and interstitial atoms. Their characteristic activation energies for crystalline aluminum are 0.54 and 2.43 eV, respectively [53]. The binding energy of a vacancy with a dislocation in aluminum is 0.181 eV [54]. Low energies are also characteristic of the bonding of vacancies with impurity atoms. For example, the binding energy of a vacancy with copper atoms is only 0.02 eV, while for silicon atoms, it is in the range 0.03–0.08 eV; for zinc atoms, 0.02–0.03 eV; and for silver atoms, it has a value of ~ 0.05–0.07 eV [55]. The activation energy for the vacancy–hydrogen-atom complex in aluminum is also relatively low and equal to 0.16 eV [56].

Features with low activation energies in the range 0.02–0.08 eV apparently do not play a significant role in the generation of the LU signals since they are already strongly excited at room temperature. In accordance with the volume of the face-centered cubic (fcc) aluminum unit cell, the activation volume Ω of the defect should be $\sim 6.6 \times 10^{-29}$m^3. It should be noted that the presented data on the nonlinear behavior of the LU signals from aluminum approximately confirm this value.

If we take the concentration of hydrogen atoms in the D16 aluminum alloy at the level of 10^{-4} to 10^{-6} of the total concentration of atoms, then considering the activation energy of the vacancy with a dislocation 0.181 eV, Eq. (28) allows us to estimate their characteristic relaxation time. To be consistent with the experimental data obtained, the relaxation time of such defects τ should be approximately $(10^5$ to $10^7)\tau_0$ at max-

imum stresses near the hole in the aluminum alloy. The known inverse Debye frequency τ_0 for aluminum is 6.5×10^{-14}s. This value is also reasonable for vacancy defects with the activation energy of 0.54 eV at room temperature if their concentration is $\sim 10^{15}$cm^{-3}. This concentration of defects is sufficient to ensure their relaxation time also at the level of 10^{-6} s for the aluminum alloy. This relaxation time is in good correspondence with the observed changes in the phase of the LU signals under the action of mechanical stresses. Therefore, at the used modulation frequencies of laser radiation, both types of defects could contribute to the LU signal.

The relations in Eqs. (27) and (29) explain the peculiarities of the LU signal dependence on stresses. For aluminum, the Fermi energy is 11.7 eV. Considering the value of Young's modulus for the D16 aluminum alloy 73 GPa and Poisson ratio $\nu \approx 0.32$, we obtain $E_F/K = 3E_F(1-2\nu)/E \approx 2.8 \times 10^{-29}$m^3. Therefore, in accordance with the relations in Eqs. (27) and (29), the signs of the coefficients b_d and b_c are different, namely, b_d is positive, and b_c is negative, in agreement with our results reported in Figs. 3 and 5.

To compare the experimental coefficients of stress dependence and the proposed model of the thermoelastic generation of ultrasound, we calculated the coefficients b and c in accordance with Eqs. (29)–(32). The results are given in Table I. The table contains the experimental coefficients b_c and c_c for the D16 aluminum alloy and b_d for silicon nitride. The coefficient c_d is not included in the table because the standard error for its fitting was too large. The reason for this is a noticeable inhomogeneity of the signal over the surface due to the grain structure of the silicon nitride ceramic. The table shows that the proposed model may describe adequately the experimental results at reasonable parameters of materials with defects. The most noteworthy fact is that the coefficient ratio c_c/b_c is determined by a single material parameter Ω, and it is equal to $k_b T_0 c_c/b_c \approx (1 \pm 0.6) \times 10^{-28}$m^3, i.e., very close to the volume of the fcc aluminum unit cell: 0.66×10^{-28}m^3.

To estimate a possible influence of strain and stress gradients on the obtained results, the coefficients b and c were estimated in two ways. First, the values of the normalized LU signals at all distances $r > a$ from the center of the hole were used for fitting. The other fitting used only the values of the original LU signals at $r > 4a$, where the hole does not affect the stress field. In this case, the stress was not high enough to reveal the nonlinear behavior of the signal. The corresponding results are also shown in Table I. The coefficients obtained by

TABLE I. Comparison of experimental and theoretical values of the coefficients b and c.

Material	Si_3N_4		D16	
Coefficient	b, GPa^{-1}	c, GPa^{-2}	b, GPa^{-1}	c, GPa^{-2}
Thermodynamic theory	0.043	0	0.34	0
Our theory	18[a]	−420[a]	−22[b]	350[b]
Nonlinear fitting of 2D distribution of the normalized LU signal	14 ± 2	–	−16 ± 7	400 ± 200
Linear fitting of the absolute LU signal far from the hole at different loads	13 ± 2	–	−16 ± 1	–

[a]The value is calculated at $n^{(d)} = 10^{18}$cm^{-3}; $U = 0.16$ eV; $\tau = 10^{-6}$s; $\tau_0 = 10^{-13}$s; $\Omega = 10^{-28}$m^3.
[b]The value is calculated at $n^{(d)} = 10^{18}$cm^{-3}; $U = 0.18$ eV; $\tau = 10^{-6}$s; $\tau_0 = 6.5 \times 10^{-14}$s; $\Omega = 6.6 \times 10^{-29}$m^3.

both methods are close. Thus, we can state that the strain and stress gradients do not significantly affect the LU signal.

VI. SUMMARY AND CONCLUSIONS

In this paper, we experimentally demonstrated different behaviors of the LU signals near a hole in stressed dielectric and conductive materials. The theoretical analysis shows that the thermodynamic approach to thermoelasticity, i.e., the approach considering only the dependence of mechanical properties of materials on temperature, is insufficient to explain the obtained experimental data on the stress dependence of thermoelastically generated ultrasound. The known models considering the stress influence only on thermophysical or elastic properties predict an effect by several orders of magnitude weaker than that observed in the experiments.

We proposed considering the excitation and relaxation of unsteady defect states as the main reason for the anomalous behavior of the LU signals in stressed materials. The nature of signal variations can be described in terms of slow dynamics with the relaxation time depending on stress. The effects of slow dynamics were previously reported by Korobov *et al.* [18] for the D16 alloy with residual stresses and rocks under dynamic loading when studying elastic properties by resonant ultrasound spectroscopy. We applied similar ideas to explain anomalous thermoelastic properties observed in the experiments.

Our main hypothesis is related to the presence of a sufficient number of defects or irregularities whose state depends on the deformation; their excitation energy is determined by the average local temperature of the ultrasound generation region. For metals, we propose additionally considering the change of the pressure of the electron gas upon the excitation of defect states. This excitation is accompanied by the temporary transition of electrons from a quasibound state to a quasifree one.

The theoretical analysis within the framework of slow dynamics explained the peculiarities of the behavior of the LU signals in strained dielectric and conductive materials. The expressions obtained for the thermal expansion coefficient correctly describe the LU signal behavior near holes under the submission to uniaxial mechanical stresses in the D16 aluminum alloy and the dielectric Si_3N_4 ceramic as typical materials with a mesoscopic structure. The coefficients of the stress dependence calculated for reasonable parameters of materials are in good agreement with the experimental data. The present approach shows that the observed nonlinear stress dependence of the LU signals can appear at the modulation frequency of laser radiation, while the generally accepted TSA thermodynamic approach predicts a quadratic stress dependence of the thermal expansion coefficient only at the second harmonic of the modulation frequency.

The presented theoretical and experimental results demonstrate that the laser method for generating ultrasonic vibrations in combination with hole drilling can be used to assess mechanical stresses in various real materials.

Further steps to study the effect of relaxation processes on the thermoelastic properties of real materials and to test the hypotheses put forward may involve expanding the list of materials with different mesoscopic structures and methods, including TSA and resonant ultrasound spectroscopy.

[1] M. C. Remillieux, R. A. Guyer, C. Payan, and T. J. Ulrich, Decoupling Nonclassical Nonlinear Behavior of Elastic Wave Types, Phys. Rev. Lett. **116**, 115501 (2016).

[2] M. Lott, M. C. Remillieux, V. Garnier, P.-Y. Le Bas, T. J. Ulrich, and C. Payan, Nonlinear elasticity in rocks: a comprehensive three-dimensional description, Phys. Rev. Mater. **1**, 023603 (2017).

[3] M. Scalerandi, C. Mechri, M. Bentahar, A. Di Bella, A. S. Gliozzi, and M. Tortello, Experimental Evidence of Correlations Between Conditioning and Relaxation in Hysteretic Elastic Media, Phys. Rev. Appl. **12**, 044002 (2019).

[4] J. A. Ten Cate, E. Smith, and R. A. Guyer, Universal Slow Dynamics in Granular Solids, Phys. Rev. Lett. **85**, 1020 (2000).

[5] P. Shokouhi, J. Rivière, R. A. Guyer, and P. A. Johnson, Slow dynamics of consolidated granular systems: multi-scale relaxation, Appl. Phys. Lett. **111**, 251604 (2017).

[6] P. Johnson and A. Sutin, Slow dynamics and anomalous nonlinear fast dynamics in diverse solids, J. Acoust. Soc. Am. **117**, 124 (2005).

[7] J. Y. Yoritomo and R. L. Weaver, Slow dynamic elastic recovery in unconsolidated metal structures, Phys. Rev. E **102**, 012901 (2020).

[8] R. Zhang and K. S. Schweize, Microscopic theory of coupled slow activated dynamics in glass-forming binary mixtures, J. Phys. Chem. B **122**, 3465 (2018).

[9] J. Y. Yoritomo and R. L. Weaver, Slow dynamic nonlinearity in unconsolidated glass bead packs, Phys. Rev. E **101**, 012901 (2020).

[10] J. Y. Yoritomo and R. L. Weaver, Slow dynamics in a single glass bead, Phys. Rev. E **101**, 012902 (2020).

[11] T. Hongo, K. Noda, S. Takagi, K. Koyama, and M. Matsuura, Dynamic properties of the intergrain glass transition in a superconductive ceramic of $YBa_2Cu_4O_8$, in *The 8th Tohwa University International Symposium on Slow Dynamics in Complex Ssystems*, edited by M. Tokuyama, AIP Conf. Proc. No. 469 (AIP, New York, 1999), p. 539.

[12] A. V. Lebedev and L. A. Ostrovsky, A unified model of hysteresis and long-time relaxation in heterogeneous materials, Acoust. Phys. **60**, 555 (2014).

[13] C. K. C. Lieou, E. G. Daub, R. E. Ecke, and P. A. Johnson, Slow dynamics and strength recovery in unconsolidated granular earth materials: a mechanistic theory, J. Geophys. Res. Solid Earth **122**, 7573 (2017).

[14] X. Li, C. Sens-Schönfelder, and R. Snieder, Nonlinear elasticity in resonance experiments, Phys. Rev. B **97**, 144301 (2018).

[15] M. Bentahar, H. El Aqra, R. Guerjouma, M. Griffa, and M. Scalerandi, Hysteretic elasticity in damaged concrete: Quantitative analysis of slow and fast dynamics, Phys. Rev. B **73**, 014116 (2006).

[16] J. A. Bittner and J. S. Popovics, Mechanistic diffusion model for slow dynamic behavior in materials, J. Mech. Phys. Solids **150**, 104355 (2021).

[17] P. Cao, M. P. Short, and S. Yip, Understanding the mechanisms of amorphous creep through molecular simulation, Proc. Natl. Acad. Sci. USA **114**, 13631 (2017).

[18] A. I. Korobov, N. I. Odina, and D. M. Mekhedov, Effect of slow dynamics on elastic properties of materials with residual and shear strains, Acoust. Phys. **59**, 387 (2013).

[19] P. A. Johnson and A. Sutin, Nonlinear elastic wave NDE I. Nonlinear resonant ultrasound spectroscopy and slow dynamics diagnostics, in *Review of Progress in Quantitative Nondestructive Evaluation*, edited by D. O. Thompson and D. E. Chimenti, AIP Conf. Proc. No. 760 (AIP, New York, 2005), p. 377.

[20] A. Astorga and P. Gueguen, Structural health building response induced by earthquakes: material softening and recovery, Eng. Reports. **2**, e12228 (2020).

[21] J. Kober, A. Kruisova, and M. Scalerandi, Elastic slow dynamics in polycrystalline metal alloys, Appl. Sci. **11**, 8631 (2021).

[22] Y. H. Pao, W. Sachse, and H. Fukuoka, Acoustoclasticity and ultrasonic measurements of residual stresses, in *Physical Acoustics*, edited by W. P. Mason and R. N. Thurston (Academic Press, New York, 1984), Vol. 17, Chap. 2, pp. 61–143.

[23] A. Karabutov, A. Devichensky, A. Ivochkin, M. Lyamshev, I. Pelivanov, U. Rohadgi, V. Solomatin, and M. Subudhi, Laser ultrasonic diagnostics of residual stress, Ultrasonics **48**, 631 (2008).

[24] K. L. Muratikov, A. L. Glazov, D. N. Rose, and J. E. Dumar, Photoacoustic effect in stressed elastic solids, J. Appl. Phys. **88**, 2948 (2000).

[25] K. L. Muratikov, A. L. Glazov, D. N. Rose, and J. E. Dumar, Photoacoustics of the stressed state in solids, Rev. Sci. Instrum. **74**, 3531 (2003).

[26] A. L. Glazov, N. F. Morozov, and K. L. Muratikov, Variations of photoacoustic signals within the Vickers indent in metals under external stresses by the examples of steel and nanocopper, Phys. Solid State **58**, 1735 (2016).

[27] A. L. Glazov, N. F. Morozov, and K. L. Muratikov, Theoretical and experimental investigation of a laser-induced photoacoustic effect near a hole in internally stressed metal plates, Phys. Mesomech. **23**, 213 (2020).

[28] H. Huan, A. Mandelis, L. Liu, and A. Melnikov, Local-stress-induced thermal conductivity anisotropy analysis using non-destructive photo-thermo-mechanical lock-in thermography (PTM-LIT) imaging, NDT Int. **91**, 79 (2017).

[29] A. F. Robinson, J. M. Dulieu-Barton, S. Quinn, and R. L. Burguete, The potential for assessing residual stress using thermoelastic stress analysis: a study of cold expanded holes, Exp. Mech. **53**, 299 (2013).

[30] A. K. Wong, R. Jones, and J. G. Sparrow, Thermoelastic constant or thermoelastic parameter? J. Phys. Chem. Solids **48**, 749 (1987).

[31] G. S. Kino and R. G. Stearns, Acoustic wave generation by thermal excitation of small regions, Appl. Phys. Lett. **47**, 926 (1985).

[32] R. G. Stearns and G. S. Kino, Effect of electronic strain on photoacoustic generation in silicon, Appl. Phys. Lett. **47**, 1048 (1985).

[33] K. L. Muratikov, A. L. Glazov, D. N. Rose, J. E. Dumar, and G. H. Quay, Photodeflection and photoacoustic microscopy of cracks and residual stresses induced by Vickers indentation in silicon nitride ceramic, Tech. Phys. Lett. **23**, 188 (1997).

[34] A. L. Glazov, N. F. Morozov, and K. L. Muratikov, The effect of external stresses on the behavior of photoacoustic signals inside Vickers indenter marks on a steel surface, Tech. Phys. Lett. **42**, 67 (2016).

[35] S. P. Timoshenko and J. N. Goodier, *Theory of Elasticity* (McGraw-Hill, New York, 1970).

[36] E. S. Folias and J. J. Wang, On the three-dimensional stress field around a circular hole in a plate of arbitrary thickness, Computat. Mech. **6**, 379 (1990).

[37] I. Tomeno, High temperature elastic moduli of Si_3N_4 ceramics, Jpn. J. Appl. Phys. **20**, 1751 (1981).

[38] G. Quinn, L. Ives, and S. Jahanmir, *On the Fractographic Analysis of Machining Cracks in Ground Ceramics: A Case Study on Silicon Nitride* (National Institute of Standards and Technology, Gaithersburg, 2003).

[39] W. Y. Li Q.Wen, W. B. Wang, F. F. Wang, Y. J. Gao, and V. Patel, Experimental and numerical investigations of bonding interface behavior in stationary shoulder friction stir lap welding, J. Mater. Sci. Technol. **35**, 192 (2019).

[40] G. Pitarresi and E. A. Patterson, A review of the general theory of thermoelastic stress analysis, J. Strain Analysis **38**, 405 (2003).

[41] O. O. Vakhnenko, V. O. Vakhnenko, T. J. Shankland, and J. A. Ten Cate, Strain-induced kinetics of intergrain defects as the mechanism of slow dynamics in the nonlinear resonant response of humid sandstone bars, Phys. Rev. E **70**, 015602(R) (2004).

[42] O. O. Vakhnenko, V. O. Vakhnenko, and T. J. Shankland, Soft-ratchet modeling of end-point memory in the nonlinear resonant response of sedimentary rocks, Phys. Rev. B **71**, 174103 (2005).

[43] S. N. Zhurkov, Kinetic concept of the strength of solids, Int. J. Fract. **1**, 311 (1965).

[44] S. N. Zhurkov and V. E. Korsukov, Atomic mechanism of fracture of solid polymers, J. Polym. Sci. Polym. Phys. Ed. **12**, 385 (1974).

[45] F. Kh. Mirzoev, V. Ya. Panchenko, and L. A. Shelepin, Laser control of processes in solids, Phys. Usp. **39**, 1 (1996).

[46] K. Trachenko, Slow dynamics and stress relaxation in a liquid as an elastic medium, Phys. Rev. B **75**, 212201 (2007).

[47] A. M. Kosevich, *Physical Mechanics of Real Crystals* (Naukova Dumka, Kiev, 1981) [in Russian].

[48] A. L. Glazov and K. L. Muratikov, Generalized thermoelastic effect in real metals and its application for describing photoacoustic experiments with Al membranes, J. Appl. Phys. **128**, 095106 (2020).

[49] A. Eisenbach, T. Havdala, J. Delahaye, T. Grenet, A. Amir, and A. Frydman1, Glassy Dynamics in Disordered Electronic Systems Reveal Striking Thermal Memory Effects, Phys. Rev. Lett. **117**, 116601 (2016).

[50] J. I. Frenkel, *Introduction to the Theory of Metals* (Nauka, Moscow, 1975) [in Russian].

[51] S. P. Ogden, T. M. Lu, and J. L. Plawsky, Electron transport and dielectric breakdown in silicon nitride using a charge transport model, Appl. Phys. Lett. **109**, 152904 (2016).

[52] S. Shao, H. Luo, L. Deng, J. He, and S. Huang, Effect of temperature on dielectric response in X-band of silicon nitride ceramics prepared by gelcasting, AIP Adv. **8**, 075127 (2018).

[53] N. Sandberg, B. Magyari-Kцpe, and T. R. Mattsson, Self-Diffusion Rates in Al from Combined First-Principles and Model-Potential Calculations, Phys. Rev. Lett. **89**, 065901 (2002).

[54] E. Clouet, The vacancy-edge dislocation interaction in fcc metals: a comparison between atomic simulations and elasticity theory, Acta Mater. **54**, 3543 (2006).

[55] C. Wolverton, Solute-vacancy binding in aluminum, Acta Mater. **55**, 5867 (2007).

[56] G. A. Young Jr., and J. R. Scully, The diffusion and trapping of hydrogen in high purity aluminum, Acta Mater. **46**, 6337 (1998).